Induced pluripotent stem cell modeling of Best disease and autosomal recessive bestrophinopathy

Ji Hwan Lee

Department of Medicine

The Graduate School, Yonsei University

Induced pluripotent stem cell modeling of Best disease and autosomal recessive bestrophinopathy

Ji Hwan Lee

Department of Medicine

The Graduate School, Yonsei University

Induced pluripotent stem cell modeling of Best disease and autosomal recessive bestrophinopathy

Directed by Professor Christopher Seungkyu Lee

The Doctoral Dissertation
submitted to the Department of Medicine,
the Graduate School of Yonsei University
in partial fulfillment of the requirements for the degree
of Doctor of Philosophy

Ji Hwan Lee

December 2019

This certifies that the Doctoral Dissertation of Ji Hwan Lee is approved.

Thesis Supervisor : Christopher Seungkyu Lee

Thesis Committee Member#1 : Sung Chul Lee

Thesis Committee Member#2 : Hee Seung Chin

Thesis Committee Member#3: Jeon Han Park

Thesis Committee Member#4: Myeong-Heon Shin

The Graduate School
Yonsei University

December 2019

ACKNOWLEDGEMENTS

I would like to express sincere gratitude to my thesis supervisor, Prof. Christopher Seungkyu Lee, who has provided generous advices, supports, and encouragements over years. I would like to appreciate Prof. Sung Chul Lee for his teaching and love. I sincerely thank Prof. Hee Seung Chin who always supports me. I would like to thank Prof. Jeon Han Park and Prof. Myeon-Heon Shin for giving me valuable advices to complete this thesis. I would also like to extend my thanks to researcher Jin Ok Oh and Dr. Yong Joon Kim for a lot of their helps and advices in experimental techniques.

I deeply thank my parents who gave birth to me and raised me with love. I would like to thank my brother Taehwan and his wife Dohee. I also appreciate my parents-in-law who always give us warm love. Finally, I thank my lovely wife Jooyeon and daughter Seungwon.

<TABLE OF CONTENTS>

LIST OF FIGURES

LIST OF TABLES

ABSTRACT

Induced pluripotent stem cell modeling of Best disease and autosomal recessive bestrophinopathy

Ji Hwan Lee

Department of Medicine
The Graduate School, Yonsei University

(Directed by Professor Christopher Seungkyu Lee)

Purpose

To understand a pathophysiology of Best disease (BD) and autosomal recessive bestrophinopathy (ARB) by establishing an *in vitro* model using human induced pluripotent stem cell (iPSC).

Methods

Human induced pluripotent stem cell (iPSC) lines were generated from mononuclear cells in peripheral blood of one autosomal recessive bestrophinopathy (ARB) patient, one autosomal dominant Best disease (BD) patient, and two normal controls. Immunocytochemistry and reverse transcriptase polymerase chain reaction in iPSC lines were conducted to demonstrate the pluripotent markers. After differentiation of iPSC into functional retinal pigment epithelium (RPE), morphological characteristics of the RPE were evaluated using confocal microscopy and immunocytochemistry. The rates of fluid flow across iPSC-RPE

monolayer were measured to compare apical to basal fluid transports by the RPE. RNA sequencing was performed on iPSC-RPE to identify the differences in gene expression profiles, and specific gene sets were tested using Gene Set Enrichment Analysis.

Results

Morphological characteristics, gene expression, and epithelial integrity of ARB iPSC were comparable to those of BD patient or normal control. Fluid transport from apical to basal was significantly decreased in ARB iPSC-RPE compared with BD iPSC-RPE or control iPSC-RPE. Gene Set Enrichment Analysis confirmed that ARB iPSC-RPE exhibited significant enrichments of epithelial-mesenchymal transition gene set and TNF-α signaling via NF-κB gene set compared with control iPSC-RPE or BD iPSC-RPE.

Conclusions

A human iPSC model of ARB showed a functional deficiency rather than anatomical defects. ARB may be caused by RPE dysfunction following BEST1 mutation.

Key words : autosomal recessive Bestrophinopathy, Best disease, induced pluripotent stem cells, retinal pigment epithelium

Induced pluripotent stem cell modeling of Best disease and autosomal recessive bestrophinopathy

Ji Hwan Lee

Department of Medicine
The Graduate School, Yonsei University

(Directed by Professor Christopher Seungkyu Lee)

I. INTRODUCTION

Hereditary retinal disease is one of the important causes of blindness, which leads to an irreversible retinal damage affecting the quality of life and daily activities. Bestrophinopathy is one of the most common inherited macular degenerations, which is caused by mutations in BEST1 gene. BEST1 is located in chromosome 11q13,[1, 2] and encodes a 585 amino acid protein known as bestrophin that localizes to the basolateral membrane of the retinal pigment epithelium (RPE).[3] When mutated, lipofuscin accumulates beneath the RPE, with degeneration of the RPE and the overlying photoreceptors.[4] The broad spectrum of clinical presentations in bestrophinopathy ranges from well-defined clinical abnormalities restricted to the macula in Best disease (BD), adult-onset foveomacular vitelliform dystrophy, or autosomal recessive bestrophinopathy (ARB) to the widespread symptoms affecting peripheral retina in a rare condition of autosomal dominant vitreoretinochoroidopathy (ADVIRC).[5, 6]

BD was first described by Friedrich Best in 1905,[7] and is most common among bestrophinopathies. It occurs in about 1 in 10000 individuals and is inherited by

autosomal dominant fashion.[6] The age at onset in BD is variable with a mean age onset in the fourth decade.[8] The macular lesion that is most characteristic of the disease is single egg-yolk-like vitelliform lesion on the central fovea, which is usually followed by vitelliruptive stage, pseudohypopyon stage, and atrophic stage.[6] A significantly decreased light rise on electrooculography (EOG) is a characteristic finding of BD.[9] Although an abnormal EOG is crucial in the diagnosis of BD in patients with vitelliform lesions, mutation analysis is necessary to confirm a clinical diagnosis of BD because 20% of patients with BEST1 mutation could have a normal EOG.[10]

ARB was first described by Burgess in 2008,[11] and is the most common juvenile macular dystrophy among bestrophinopathies. ARB is an autosomal recessive disease caused by homozygous or compound heterozygous mutations in the BEST1 gene.[6] Nearly 40 biallelic mutations in BEST1 have been reported in ARB patients at present.[12-28] The retinopathy includes an irregularity of the RPE throughout the posterior fundus with punctate flecks, which is easily seen on autofluorescence imaging. Retinal edema and subretinal fluid are common findings on OCT imaging. ARB shows markedly abnormal EOG and pattern electroretinography (ERG).[11]

Human induced pluripotent stem cells (iPSC) are relatively non-invasive and renewable, and iPSC-derived models can recapitulate cellular and molecular processes without genetic manipulation.[29] The retina and the brain are promising candidates for iPSC modeling since it is difficult to perform biopsy in these tissues and there are established preexisting protocols to isolate their progenitors from iPSC.[30-32] The RPE can be readily differentiated and re-seeded widely, which is a promising candidate for iPSC modeling. In this study, we established an *in vitro* model of BD and ARB using human iPSC to understand a pathophysiology.

II. MATERIALS AND METHODS

1. Differentiation of human iPSC lines

A. Generation of iPSC lines

Twenty milliliters peripheral blood were obtained from one ARB patient (L40P and A195V mutations in BEST1 gene), one autosomal dominant BD patient (G96A mutation in BEST1 gene), and two normal controls. Human iPSC lines were generated using previously established methods.[30, 31] Mononuclear cells (MNC) were isolated from the blood samples and were expanded in MNC media for 7-10 days.

MNC were transfected with episomal vectors (OCT4, SOX2, c-MYC, KLF4, LIN28) (Thermo Fisher Scientific, Waltham, MA, USA) and cultured on extracellular matrices (BD, Franklin Lakes, NJ, USA). Culture on iPSC medium (STEMCELL Technologies, Vancouver, Canada) were performed for 1-2 weeks till colonization of iPSC. iPSC colonies were isolated and expanded on iPSC medium (STEMCELL Technologies). Differentiation was initiated after 10-20 passages of expansion to remove an epigenetic memory.

B. Differentiation of iPSC into functional RPE cell

Embryoid body (EB) was formed for one week on EB media (Thermo Fisher Scientific) and free-floating culture. EB was then switched to a chemically defined neural induction media (Thermo Fisher Scientific) and laminin-coated plate (Thermo Fisher Scientific) for 10 days for neural differentiation. For retinal differentiation, iPSC-derived neuroepithelial rosettes were switched to a chemically defined retinal differentiation medium (Thermo Fisher Scientific).

2. RT-PCR

Total RNA was isolated from cell cultures from various stages of differentiation and treated with DNase I (Thermo Fisher Scientific). cDNA was synthesized using the SuperScript III RT-PCR kit (Thermo Fisher Scientific). Samples were denatured at 95℃ for 5 minutes followed by 30 cycles of PCR amplification (95℃ for 15 seconds, 60℃ for 30 seconds, 72℃ for 1 minute) and a final extension at 72℃ for 10 minutes. PCR products were run on 2% agarose gel.

3. Immunocytochemistry

Cells were washed in ice-cold phosphate-buffered saline (PBS) and fixed in 2-4% paraformaldehyde at 4℃ for 30 minutes. Fixed cells were washed twice in PBS and placed in blocking solution (10% normal donkey or goat serum and 0.01-0.05% Triton-X100 in PBS) for 1 hour at room temperature. Cells were then incubated overnight at 4℃ with mouse anti-BEST1 monoclonal antibody (E6-6) (Thermo Fisher Scientific) and rabbit anti-ZO-1 polyclonal antibody (Thermo Fisher Scientific). The following day, cells were washed three to five times in PBS with 0.01% Triton-X100 and incubated with Alexa Fluor 488-conjugated goat anti-rabbit antibody (Thermo Fisher Scientific) and Alexa Fluor 568-conjugated donkey anti-rabbit antibody (Thermo Fisher Scientific). After secondary antibody incubation, cells were stained with DAPI (Thermo Fisher Scientific), washed three times in PBS with 0.2% Triton-X100, and imaged on a confocal microscope (Zeiss, Jena, Germany).

4. Transepithelial resistance (TER) measurement

TER of RPE monolayers cultured on permeable transwell filters (Merck KGaA, Darmstadt, Germany) was measured using an epithelial voltohmmeter (Merck KGaA) according to manufacturer’s instructions. Electrodes were sterilized with 70% ethanol and rinsed in Hank’s balanced salt solution prior to placement

in the transwell inserts. Net TER was calculated by subtracting the background measurement obtained from transwell filters and multiplying the difference by the area of the transwell filter ($\Omega*cm^2$).

5. Measurement of fluid flux

The quantification of active fluid transport from apical to basal side in the RPE was measured using a previously described method.[33] A fixed amount of medium (Thermo Fisher Scientific), 150 µl in the apical and 400 µl in the basal chambers of transwell was loaded. The amount of fluid remaining in the apical chamber was measured 20 hours later, and the rate of fluid transport was calculated ($\mu l/hr/cm^2$).

6. RNA sequencing and data analysis

RNA sequencing was performed on ARB iPSC-RPE, BD iPSC-RPE, and normal iPSC-RPE (n=2 for each) by the Macrogen (Seoul, Korea). Total RNA quality was assessed with Agilent bioanalyzer system (Agilent, Santa Clara, CA, USA). Extracted RNA samples were processed with TruSeq Stranded Total RNA Prep Kit (Illumina, San Diego, CA, USA) and sequenced on NovaSeq 6000 system (Illumina). A median 1.2×10^8 single-end reads (range, 1.1×10^8 to 1.3×10^8) with 101 base pairs were generated. Reads were trimmed base on sequencing quality using Trimmomatic (RWTH Aachen University, Aachen, Germany).[34] Trimmed reads were aligned on a human reference sequence (hg19) using HISAT2 (Johns Hopkins University, Baltimore, USA).[35] Using Gene Set Enrichment Analysis, an enrichment of a specific gene set was tested, and core enrichment genes were determined.[36]

7. Statistical analysis

All statistical analyses were performed using SPSS version 23.0 (IBM, Chicago, IL, USA). The Shapiro-Wilk test was used to assess distribution patterns of data. TER measurement and the rate of fluid flow obtained from ARB iPSC-RPE were compared with those of control and BD iPSC-RPE using the Mann-Whitney test. A p-value of <0.05 was considered statistically significant.

III. RESULTS

1. Clinical findings

Demographic and characteristics of patient with Best vitelliform macular dystrophy and patient with ARB were summarized in Table 1. Patient 1 was a 41-year-old woman with decreased visual acuity in the right eye. Her best-corrected visual acuity was 20/40 in the right eye and 20/20 in the left eye. The patient was hyperopic with spherical equivalent +1.75 diopter (OD) and +1.00 diopter (OS). The fundus showed RPE atrophy and pigment disruption in the right eye and a dome-shaped accumulation of yellowish material in the central macula of the left eye (Figure 1A and 1B). Hyperreflective vitelliform materials with subretinal fluid were found in the subretinal space on OCT images (Figure 1C and 1D). EOG showed decreased response with Arden ratio 1.1 in both eyes.

Patient 2 was a 57-year-old woman who reported significant visual loss in both eyes at the age of 20 years. She presented with a further decrease of the visual acuity in her left eye for two months. Her visual acuity was 20/400 in the right eye and 20/800 in the left eye. The patient was hyperopic with spherical equivalent +3.00 diopter (OD) and +3.25 diopter (OS). The fundus showed

bilateral RPE irregularities in the posterior pole with scattered yellowish flecks (Figure 2A and 2B), which were more prominent on autofluorescence images. A neurosensory retinal detachment with subretinal fluid was observed in the left eye on an OCT image, which appeared similar to that of the fellow eye (Figure 2C). Electrophysiology showed normal response for the full-field ERG, but a light rise on EOG was absent (Arden ratio 1.0) in both eyes.

Table 1. Demographics and Characteristics of Patients and Normal Controls.

Patient	Sex	Age	Diagnosis	ERG	EOG	Inheritance	BEST1 mutation	Amino acid change
NL 1	F	46	NL control	NL	NL	NA	NA	NA
NL 2	M	44	NL control	NL	NL	NA	NA	NA
Patient 1	F	41	BD	NL	Flat	AD	c.287A>G	Gln96Arg
Patient 2	F	57	ARB	NL	Flat	AR	c.119T>C c.584C>T	Leu40Pro Ala195Val

AD: autosomal dominant, AR: autosomal recessive, ARB: autosomal recessive bestrophinopathy, BD: Best disease, EOG: electrooculography, ERG: electroretinography, NA: not applicable, NL: normal

Figure 1. Clinical findings of patient 1. A 41-year-old woman presented with decreased visual acuity in the right eye. (A, B) Color fundus photography showed RPE atrophy and pigment disruption in the right eye and a dome-shaped accumulation of yellowish material in the central macula of the left eye. (C, D) Hyperreflective materials with subretinal fluid were found in the subretinal space on optical coherence tomographic images.

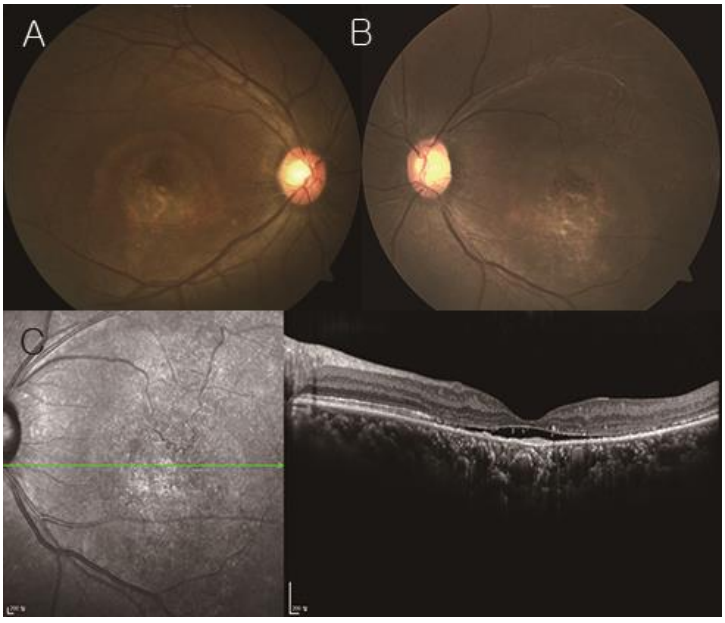

Figure 2. Clinical findings of patient 2. A-57-year-old woman presented with decreased visual acuity in her left eye for two months. She had reported significant visual loss in both eyes at the age of 20 years. (A, B) Color fundus photography showed bilateral RPE irregularities in the posterior pole with scattered yellowish flecks. (C) A neurosensory retinal detachment with subretinal fluid was observed in the left eye on an optical coherence tomography image, which appeared similar to that of the fellow eye.

2. Generation of iPSC lines

Mononuclear cells were isolated from peripheral blood and iPSC lines were generated using previously established methods.[30, 31] Immunocytochemistry and RT-PCR in iPSC lines were performed to confirm the pluripotent markers. Immunocytochemistry analysis using confocal microscopy demonstrated that all iPSC lines expressed the pluripotent markers including OCT4, SOX2, TRA-1-60, and SSEA4 (Figure 3). RT-PCR revealed pluripotency markers including c-MYC, OCT4, SOX2, NANOG, and KLF4 (Figure 4), and teratoma studies confirmed that 7-day embryoid bodies derived from iPSC showed markers for all three lineages (Figure 5).

3. Differentiation of iPSC into RPE cell

Light microscopy and RT-PCR were performed to confirm the differentiation of iPSC into RPE cell. RPE differentiation was performed in retinal differentiation media until approximately Day 40-90, at which characteristic polygonality and pigmentation of the RPE could be confirmed on light microscopy (Figure 6A). RT-PCR revealed the expressions of a characteristic RPE gene BEST1 and a tight junction gene OCCLUDIN (Figure 6B).

4. Cytological and functional analysis of ARB iPSC-RPE

Morphological characteristics of the RPE were evaluated using confocal microscopy and immunocytochemistry. The rate of fluid flow across iPSC-RPE monolayer on transwell insert was measured to compare apical to basal fluid transports by the RPE. Immunocytochemistry revealed uniform tight junction protein ZO-1 in both ARB and control iPSC-RPE (Figure 7). There was no significant difference in TER measurements between ARB patient, autosomal dominant BD patient, and normal control. TER measurements obtained from

ARB iPSC-RPE (290.00±10.24 Ω) were similar to those of BD iPSC-RPE (312.67±23.84 Ω, p=0.936) and control iPSC-RPE (305.83±13.33 Ω, p=0.335) (Figure 8A). The rate of fluid flow was the lowest in ARB iPSC-RPE (0.12±0.01) and was significantly lower than those of control iPSC-RPE (0.35±0.02, p<0.001) and BD iPSC-RPE (0.29±0.02, p<0.001) (Figure 8B).

5. Gene expression profiles of ARB iPSC-RPE

RNA-sequencing was performed to identify the differences in gene expression profiles between ARB iPSC-RPE, BD iPSC-RPE, and control iPSC-RPE. Gene Set Enrichment Analysis showed that ARB iPSC-RPE exhibited significant enrichment of epithelial-mesenchymal transition (EMT) gene set compared with control iPSC-RPE (Figure 9A). Genes encoding TNF-α signaling via NF-κB were also significantly enriched in ARB iPSC-RPE compared with control iPSC-RPE (Figure 9B). ARB iPSC-RPE showed similar results compared with BD iPSC-RPE (Figure 9C and 9D).

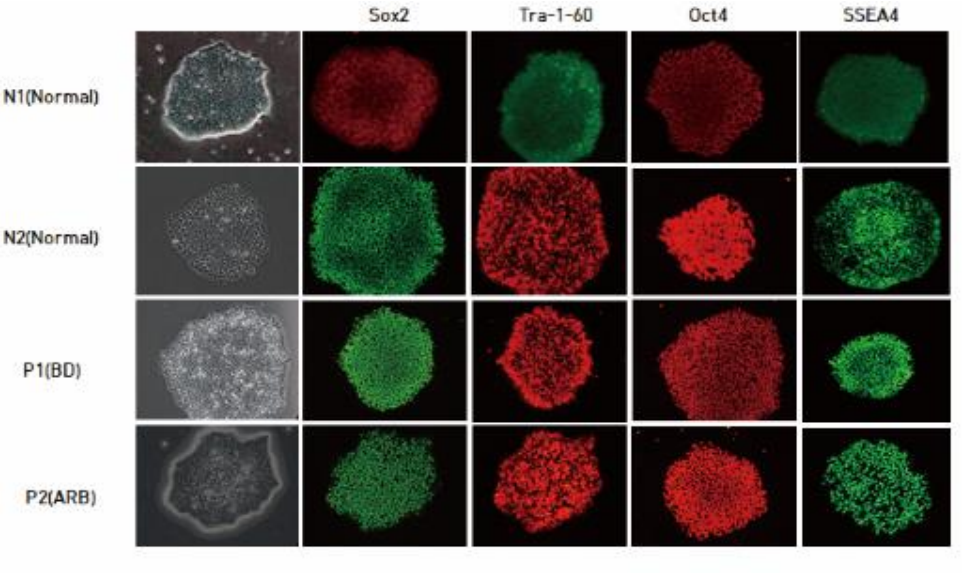

Figure 3. Immunocytochemistry in iPSC lines. Immunocytochemistry analysis demonstrated the expression of pluripotency markers (OCT4, SOX2, TRA1-60, and SSEA4) in all iPSC lines of normal controls and patients.

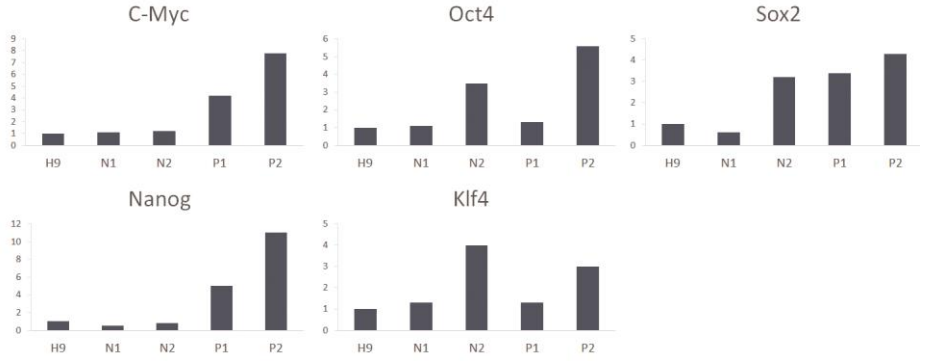

Figure 4. RT-PCR in iPSC lines. RT-PCR revealed mRNA expression of pluripotency markers (c-MYC, OCT4, SOX2, NANOG, and KLF4) in undifferentiated iPSC lines from normal controls and patients. Human embryonic stem cells (H9) were used as a positive control.

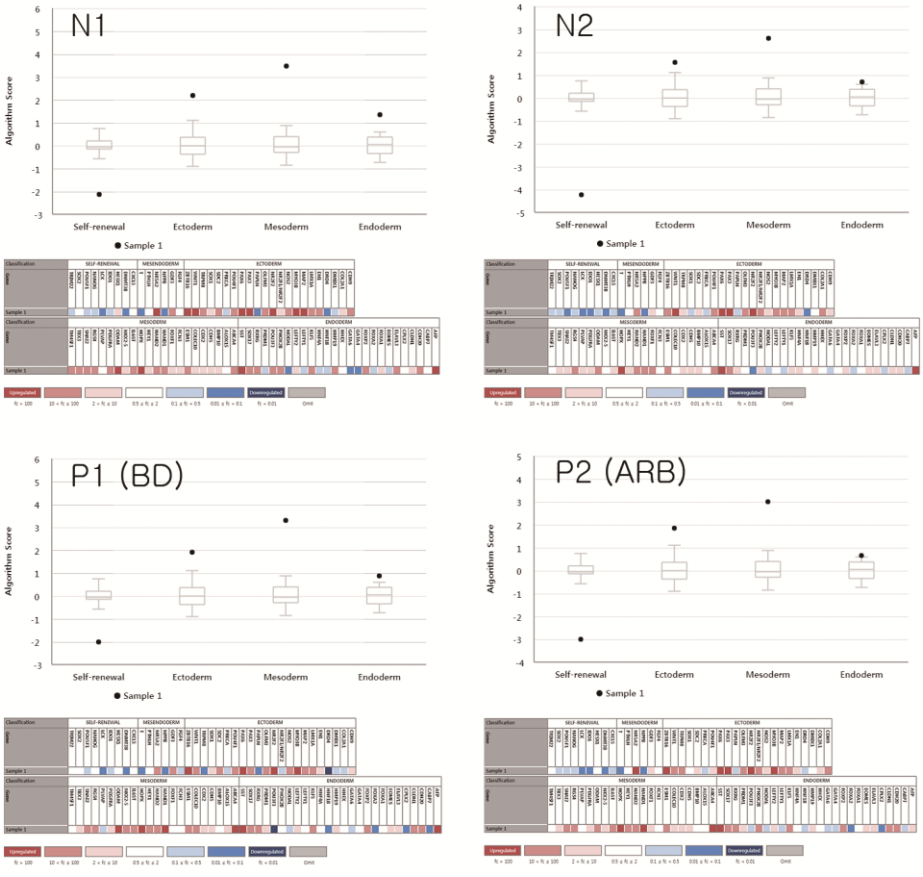

Figure 5. Teratoma analyses of iPSC lines. Teratoma studies from normal controls and patients demonstrated derivatives from the endodermal, ectodermal, and mesodermal germ lineages.

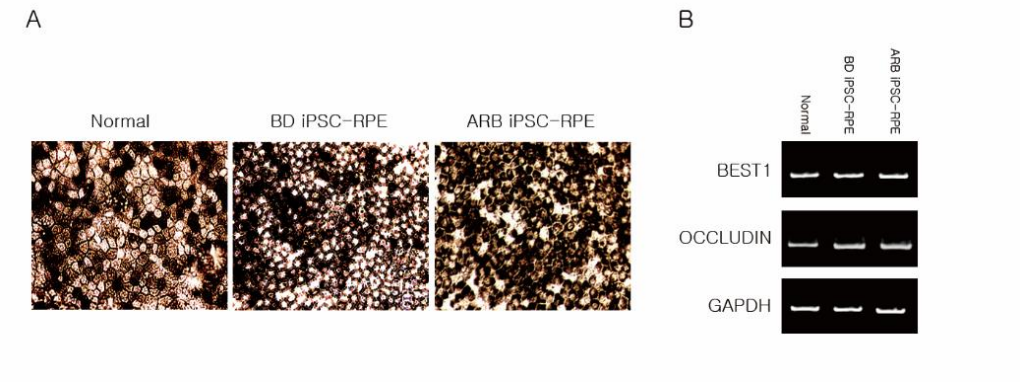

Figure 6. Differentiation of induced pluripotent stem cells into functional retinal pigment epithelium (RPE) cells. (A) Characteristic polygonality and pigmentation of the RPE could be confirmed using light microscopy. (B) RT-PCR revealed the expressions of a characteristic RPE gene BEST1 and a tight junction gene OCCLUDIN. GAPDH was as a loading control.

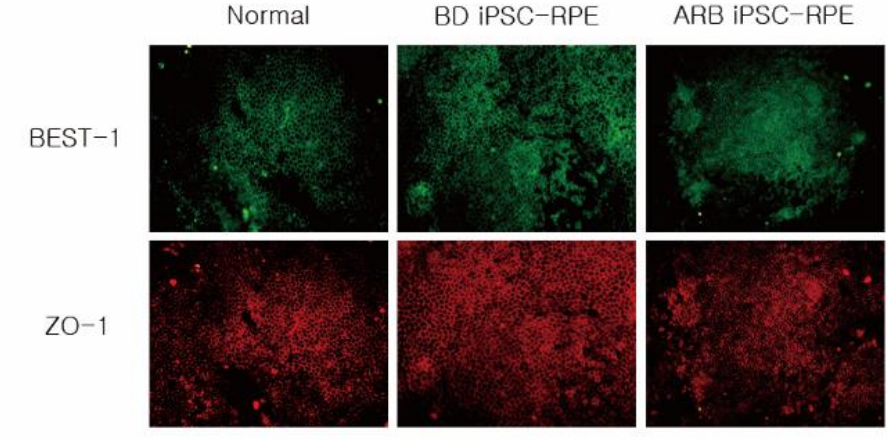

Figure 7. Immunocytochemistry in iPSC-RPE. Immunocytochemistry for BEST1 and ZO-1 showed uniform morphology and tight junction in Best disease, ARB and control iPSC-RPE.

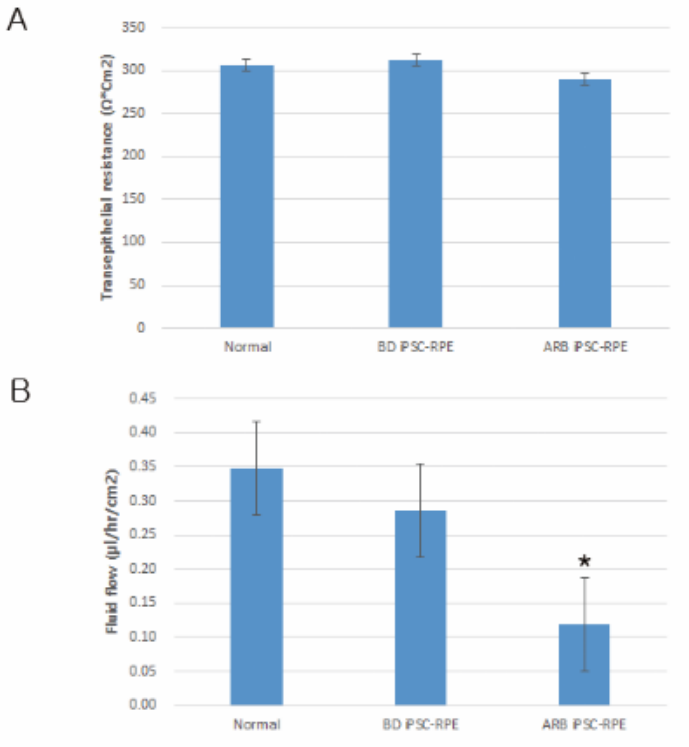

Figure 8. Transepithelial resistance (TER) measurements and the quantification of fluid movement in BD iPSC-RPE, ARB iPSC-RPE, and control iPSC-RPE. (A) TER were comparable between patients and control iPSC-RPE. (B) The rate of fluid flow was the lowest in ARB iPSC-RPE and was significantly lower than those of control iPSC-RPE and BD iPSC-RPE. *$p<0.001$ compared with control or BD iPSC-RPE.

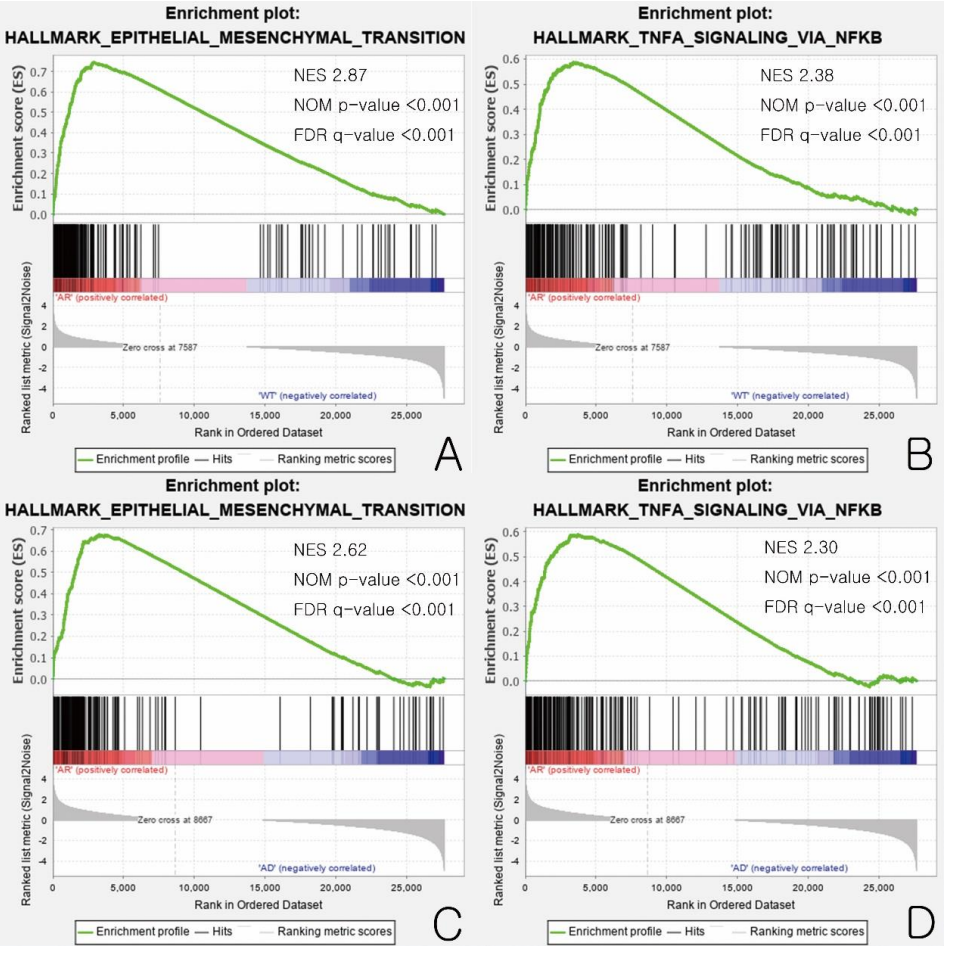

Figure 9. Gene Set Enrichment Analysis (GSEA). GSEA plots showed that epithelial-mesenchymal transition gene set and TNF-α signaling via NF-κB gene set were significantly enriched in ARB iPSC-RPE compared with control iPSC-RPE (A, B) or BD iPSC-RPE (C, D). FDR: false discovery rate, NES: normalized enrichment score, NOM: nominal

IV. DISCUSSION

In this study, a human iPSC model of ARB was evaluated to understand its pathophysiology, which revealed a functional deficiency rather than anatomical defects. Morphological characteristics, gene expression, and epithelial integrity of ARB iPSC were comparable to those of normal control. Fluid transport from apical to basal was more reduced in ARB iPSC-RPE than in autosomal dominant BD iPSC-RPE.

RPE-based disorders appear to be ideal for human iPSC modeling given the ease and extent to which this cell type can be generated, manipulated and tested. The maturation state of iPSC-RPE can be also monitored in live cultures using morphological features and measurement of transepithelial resistance.[37] Singh et al developed a iPSC-RPE model of Best vitelliform macular dystrophy utilizing these characteristics of human RPE. They demonstrated that RPE from mutant iPSC displayed disrupted fluid flux and increased accrual of autofluorescent material after long-term photoreceptor outer segment feeding.[29] Thus, human iPSC-derived RPE is a potentially useful tool for disease modeling and therapeutics in human retinal degenerative diseases.

Defect in transcellular fluid in iPSC-RPE was more prominent in ARB patient than in autosomal dominant BD patient, which could explain common macular edema and subretinal fluid in ARB patient. The macular pathology in BD patients usually seems to be stable until the late stage of the disease course, and most patients retain moderate visual acuity until late in life.[38, 39] Thus, the result may also support that BD is caused by the cumulative effects of one or more subtle alterations in RPE physiology. Other cytological examinations including morphological characteristics, gene expression, and epithelial integrity revealed similar results between ARB iPSC-RPE and normal control. Considering more prominent defect in transcellular fluid in ARB iPSC-RPE than in autosomal

dominant BD iPSC-RPE, these findings may suggest that ARB is caused by BEST1 dysfunction.

EMT is a biologic process resulting in the conversion of epithelial cells to myofibroblasts.[40, 41] It is characterized by the loss of epithelial characteristics which includes apical-basolateral polarity and cell-cell adhesions.[42] Increased expression of transforming growth factor-β, α-smooth muscle actin, extracellular matrix proteins collagen type 1, matrix metalloproteinases induces this process.[40, 42-44] EMT of the RPE is known to be related to the pathogenesis of subretinal fibrosis in various retinal diseases including age-related macular degeneration.[45-47] NF-κB activation by TNF-α is well-known to play a crucial role in EMT.[48-51] Recently, an association between EMT genes and genes involved in NF-κB activation has been reported.[50,52,53] Gene expression profiles of ARB iPSC-RPE exhibited significant enrichment of epithelial-mesenchymal transition gene set compared with control iPSC-RPE or BD iPSC-RPE. Genes encoding TNF-α signaling via NF-κB were also enriched in ARB iPSC-RPE compared with control iPSC-RPE or BD iPSC-RPE. Thus, these results indicate that inhibiting EMT and NF-κB activation in the RPE could be a potential therapeutic target for ARB.

The lack of peripheral retinal findings in BD and ARB is possibly related to the capacity for RPE cells to withstand the presence of dysfunctional BEST1. This difference in phenotype between central and peripheral retina in BD and ARB could be explained by regional differences in the RPE or superimposed environmental stress upon the macular RPE.[29] Further studies are necessary to evaluate whether iPSC-RPE cells are more similar to macula or peripheral retina.

V. CONCLUSION

This study established an in vitro model of ARB which showed a functional deficiency rather than anatomical defects. Fluid transport from apical to basal was significantly reduced in ARB iPSC-RPE compared to that of autosomal dominant BD iPSC-RPE. ARB may be caused by RPE dysfunction following BEST1 mutation.

Table 2. Transepithelial Resistance Measurement and the Rate of Fluid Flow in BD iPSC-RPE and ARB iPSC-RPE.

	Control	BD iPSC-RPE	p-value	ARB iPSC-RPE	p-value
TER (Ω*cm^2)	305.83±13.33	312.67±23.84	0.936	290.00±10.24	0.335
Fluid flow (μl/hr/cm^2)	0.35±0.02	0.29±0.02	0.038	0.12±0.01	0.000

ARB iPSC-RPE: autosomal recessive induced pluripotent stem cell retinal pigment epithelium, BD iPSC-RPE: autosomal dominant induced pluripotent stem cell retinal pigment epithelium, TER: transepithelial resistance

REFERENCES

1. Forsman K, Graff C, Nordstrom S, Johansson K, Westermark E, Lundgren E, et al. The gene for Best's macular dystrophy is located at 11q13 in a Swedish family. Clin Genet. 1992;42:156-9.

2. Stone EM, Nichols BE, Streb LM, Kimura AE, Sheffield VC. Genetic linkage of vitelliform macular degeneration (Best's disease) to chromosome 11q13. Nat Genet. 1992;1:246-50.

3. Marmorstein AD, Marmorstein LY, Rayborn M, Wang X, Hollyfield JG, Petrukhin K. Bestrophin, the product of the Best vitelliform macular dystrophy gene (VMD2), localizes to the basolateral plasma membrane of the retinal pigment epithelium. Proceedings of the National Academy of Sciences of the United States of America. 2000;97:12758-63.

4. O'Gorman S, Flaherty WA, Fishman GA, Berson EL. Histopathologic findings in Best's vitelliform macular dystrophy. Arch Ophthalmol. 1988;106:1261-8.

5. Guziewicz KE, Sinha D, Gomez NM, Zorych K, Dutrow EV, Dhingra A, et al. Bestrophinopathy: An RPE-photoreceptor interface disease. Prog Retin Eye Res. 2017;58:70-88.

6. Boon CJ, Klevering BJ, Leroy BP, Hoyng CB, Keunen JE, den Hollander AI. The spectrum of ocular phenotypes caused by mutations in the BEST1 gene. Prog Retin Eye Res. 2009;28:187-205.

7. Friedrich B. Über eine hereditäre Maculaaffektion. Beitrag zur Vererbungslehre. Z Augenheilk. 1905;13:199-212.

8. Renner AB, Tillack H, Kraus H, Kramer F, Mohr N, Weber BH, et al. Late

onset is common in best macular dystrophy associated with VMD2 gene mutations. Ophthalmology. 2005;112:586-92.

9. Deutman AF. Electro-oculography in families with vitelliform dystrophy of the fovea. Detection of the carrier state. Arch Ophthalmol. 1969;81:305-16.

10. Meunier I, Senechal A, Dhaenens CM, Arndt C, Puech B, Defoort-Dhellemmes S, et al. Systematic screening of BEST1 and PRPH2 in juvenile and adult vitelliform macular dystrophies: a rationale for molecular analysis. Ophthalmology. 2011;118:1130-6.

11. Burgess R, Millar ID, Leroy BP, Urquhart JE, Fearon IM, De Baere E, et al. Biallelic mutation of BEST1 causes a distinct retinopathy in humans. American journal of human genetics. 2008;82:19-31.

12. Lee CS, Jun I, Choi SI, Lee JH, Lee MG, Lee SC, et al. A Novel BEST1 Mutation in Autosomal Recessive Bestrophinopathy. Invest Ophthalmol Vis Sci. 2015;56:8141-50.

13. Gerth C, Zawadzki RJ, Werner JS, Heon E. Detailed analysis of retinal function and morphology in a patient with autosomal recessive bestrophinopathy (ARB). Doc Ophthalmol. 2009;118:239-46.

14. Davidson AE, Sergouniotis PI, Burgess-Mullan R, Hart-Holden N, Low S, Foster PJ, et al. A synonymous codon variant in two patients with autosomal recessive bestrophinopathy alters in vitro splicing of BEST1. Mol Vis. 2010;16:2916-22.

15. Guerriero S, Preising MN, Ciccolella N, Causio F, Lorenz B, Fischetto R. Autosomal recessive bestrophinopathy: new observations on the retinal phenotype - clinical and molecular report of an Italian family. Ophthalmologica

Journal international d'ophtalmologie International journal of ophthalmology Zeitschrift fur Augenheilkunde. 2011;225:228-35.

16. Iannaccone A, Kerr NC, Kinnick TR, Calzada JI, Stone EM. Autosomal recessive best vitelliform macular dystrophy: report of a family and management of early-onset neovascular complications. Arch Ophthalmol. 2011;129:211-7.

17. Kinnick TR, Mullins RF, Dev S, Leys M, Mackey DA, Kay CN, et al. Autosomal recessive vitelliform macular dystrophy in a large cohort of vitelliform macular dystrophy patients. Retina. 2011;31:581-95.

18. Pineiro-Gallego T, Alvarez M, Pereiro I, Campos S, Sharon D, Schatz P, et al. Clinical evaluation of two consanguineous families with homozygous mutations in BEST1. Mol Vis. 2011;17:1607-17.

19. Wittstrom E, Ekvall S, Schatz P, Bondeson ML, Ponjavic V, Andreasson S. Morphological and functional changes in multifocal vitelliform retinopathy and biallelic mutations in BEST1. Ophthalmic genetics. 2011;32:83-96.

20. MacDonald IM, Gudiseva HV, Villanueva A, Greve M, Caruso R, Ayyagari R. Phenotype and genotype of patients with autosomal recessive bestrophinopathy. Ophthalmic genetics. 2012;33:123-9.

21. Pomares E, Bures-Jelstrup A, Ruiz-Nogales S, Corcostegui B, Gonzalez-Duarte R, Navarro R. Nonsense-mediated decay as the molecular cause for autosomal recessive bestrophinopathy in two unrelated families. Invest Ophthalmol Vis Sci. 2012;53:532-7.

22. Zhao L, Grob S, Corey R, Krupa M, Luo J, Du H, et al. A novel compound heterozygous mutation in the BEST1 gene causes autosomal recessive Best

vitelliform macular dystrophy. Eye. 2012;26:866-71.

23. Boon CJ, van den Born LI, Visser L, Keunen JE, Bergen AA, Booij JC, et al. Autosomal recessive bestrophinopathy: differential diagnosis and treatment options. Ophthalmology. 2013;120:809-20.

24. Crowley C, Paterson R, Lamey T, McLaren T, De Roach J, Chelva E, et al. Autosomal recessive bestrophinopathy associated with angle-closure glaucoma. Doc Ophthalmol. 2014;129:57-63.

25. Fung AT, Yzer S, Goldberg N, Wang H, Nissen M, Giovannini A, et al. New best1 mutations in autosomal recessive bestrophinopathy. Retina. 2015;35:773-82.

26. Nakanishi A, Ueno S, Hayashi T, Katagiri S, Kominami T, Ito Y, et al. Clinical and Genetic Findings of Autosomal Recessive Bestrophinopathy in Japanese Cohort. Am J Ophthalmol. 2016;168:86-94.

27. Wivestad Jansson R, Berland S, Bredrup C, Austeng D, Andreasson S, Wittstrom E. Biallelic Mutations in the BEST1 Gene: Additional Families with Autosomal Recessive Bestrophinopathy. Ophthalmic genetics. 2016;37:183-93.

28. Luo J, Lin M, Guo X, Xiao X, Li J, Hu H, et al. Novel BEST1 mutations and special clinical characteristics of autosomal recessive bestrophinopathy in Chinese patients. Acta ophthalmologica. 2019;97:247-59.

29. Singh R, Shen W, Kuai D, Martin JM, Guo X, Smith MA, et al. iPS cell modeling of Best disease: insights into the pathophysiology of an inherited macular degeneration. Human molecular genetics. 2013;22:593-607.

30. Meyer JS, Shearer RL, Capowski EE, Wright LS, Wallace KA, McMillan

EL, et al. Modeling early retinal development with human embryonic and induced pluripotent stem cells. Proceedings of the National Academy of Sciences of the United States of America. 2009;106:16698-703.

31. Meyer JS, Howden SE, Wallace KA, Verhoeven AD, Wright LS, Capowski EE, et al. Optic vesicle-like structures derived from human pluripotent stem cells facilitate a customized approach to retinal disease treatment. Stem Cells. 2011;29:1206-18.

32. Phillips MJ, Wallace KA, Dickerson SJ, Miller MJ, Verhoeven AD, Martin JM, et al. Blood-derived human iPS cells generate optic vesicle-like structures with the capacity to form retinal laminae and develop synapses. Invest Ophthalmol Vis Sci. 2012;53:2007-19.

33. Stamer WD, Bok D, Hu J, Jaffe GJ, McKay BS. Aquaporin-1 channels in human retinal pigment epithelium: role in transepithelial water movement. Invest Ophthalmol Vis Sci. 2003;44:2803-8.

34. Bolger AM, Lohse M, Usadel B. Trimmomatic: a flexible trimmer for Illumina sequence data. Bioinformatics. 2014;30:2114-20.

35. Kim D, Paggi JM, Park C, Bennett C, Salzberg SL. Graph-based genome alignment and genotyping with HISAT2 and HISAT-genotype. Nature biotechnology. 2019;37:907-15.

36. Subramanian A, Tamayo P, Mootha VK, Mukherjee S, Ebert BL, Gillette MA, et al. Gene set enrichment analysis: a knowledge-based approach for interpreting genome-wide expression profiles. Proceedings of the National Academy of Sciences of the United States of America. 2005;102:15545-50.

37. Gamm DM, Phillips MJ, Singh R. Modeling retinal degenerative diseases

with human iPS-derived cells: current status and future implications. Expert review of ophthalmology. 2013;8:213-6.

38. Fishman GA, Baca W, Alexander KR, Derlacki DJ, Glenn AM, Viana M. Visual acuity in patients with best vitelliform macular dystrophy. Ophthalmology. 1993;100:1665-70.

39. Ponjavic V, Eksandh L, Andreasson S, Sjostrom K, Bakall B, Ingvast S, et al. Clinical expression of Best's vitelliform macular dystrophy in Swedish families with mutations in the bestrophin gene. Ophthalmic genetics. 1999;20:251-7.

40. Kalluri R, Neilson EG. Epithelial-mesenchymal transition and its implications for fibrosis. The Journal of clinical investigation. 2003;112:1776-84.

41. Kobayashi M, Tokuda K, Kobayashi Y, Yamashiro C, Uchi SH, Hatano M, et al. Suppression of Epithelial-Mesenchymal Transition in Retinal Pigment Epithelial Cells by an MRTF-A Inhibitor. Invest Ophthalmol Vis Sci. 2019;60:528-37.

42. Mamuya FA, Duncan MK. aV integrins and TGF-beta-induced EMT: a circle of regulation. J Cell Mol Med. 2012;16:445-55.

43. Tan TK, Zheng G, Hsu TT, Wang Y, Lee VW, Tian X, et al. Macrophage matrix metalloproteinase-9 mediates epithelial-mesenchymal transition in vitro in murine renal tubular cells. The American journal of pathology. 2010;176:1256-70.

44. Moustakas A, Heldin P. TGFbeta and matrix-regulated epithelial to mesenchymal transition. Biochim Biophys Acta. 2014;1840:2621-34.

45. Friedlander M. Fibrosis and diseases of the eye. The Journal of clinical investigation. 2007;117:576-86.

46. Tamiya S, Kaplan HJ. Role of epithelial-mesenchymal transition in proliferative vitreoretinopathy. Experimental eye research. 2016;142:26-31.

47. Ishikawa K, Kannan R, Hinton DR. Molecular mechanisms of subretinal fibrosis in age-related macular degeneration. Experimental eye research. 2016;142:19-25.

48. Bates RC, Mercurio AM. Tumor necrosis factor-alpha stimulates the epithelial-to-mesenchymal transition of human colonic organoids. Mol Biol Cell. 2003;14:1790-800.

49. Huber MA, Azoitei N, Baumann B, Grunert S, Sommer A, Pehamberger H, et al. NF-kappaB is essential for epithelial-mesenchymal transition and metastasis in a model of breast cancer progression. The Journal of clinical investigation. 2004;114:569-81.

50. Maier HJ, Schmidt-Strassburger U, Huber MA, Wiedemann EM, Beug H, Wirth T. NF-kappaB promotes epithelial-mesenchymal transition, migration and invasion of pancreatic carcinoma cells. Cancer Lett. 2010;295:214-28.

51. Li CW, Xia W, Huo L, Lim SO, Wu Y, Hsu JL, et al. Epithelial-mesenchymal transition induced by TNF-alpha requires NF-kappaB-mediated transcriptional upregulation of Twist1. Cancer Res. 2012;72:1290-300.

52. Chung CH, Parker JS, Ely K, Carter J, Yi Y, Murphy BA, et al. Gene expression profiles identify epithelial-to-mesenchymal transition and activation of nuclear factor-kappaB signaling as characteristics of a high-risk head and

neck squamous cell carcinoma. Cancer Res. 2006;66:8210-8.

53. Pires BR, Mencalha AL, Ferreira GM, de Souza WF, Morgado-Diaz JA, Maia AM, et al. NF-kappaB Is Involved in the Regulation of EMT Genes in Breast Cancer Cells. PloS one. 2017;12:e0169622.

ABSTRACT(IN KOREAN)

역분화줄기세포를 이용한 베스트병과 열성유전베스트병 질명모델의 구축

<지도교수 이승규>

연세대학교 대학원 의학과

이지환

목적: 인간 역분화줄기세포를 이용하여 베스트병과 열성유전베스트병의 체외모델을 구축하고자 함.

방법: 열성유전베스트병 환자 1명과 우성유전베스트병 환자 1명, 정상 대조군 2명으로부터 채취한 말초혈액샘플에서 인간 역분화줄기세포주를 생성하였다. 만능성 표지자를 역분화줄기세포주에서 확인하기 위해 면역세포화학염색과 역전사 중합효소 연쇄반응을 시행하였다. 역분화줄기세포를 망막색소상피로 분화한 후, 공초점 현미경과 면역세포화학염색을 사용하여 망막색소상피의 형태학적 특성을 분석하였다. 역분화줄기세포에 대하여 RNA 염기순서분석을 시행하고, 구체적 유전자 집합에 대하여 유전자 집합 농축 분석을 실시하였다.

결과: 열성유전베스트병 역분화줄기세포의 형태학적 특성과 유전자 발현, 상피 피완전성은 베스트병 환자 혹은 정상 대조군 역분화줄기세포와 비교하여 유사한 소견을 보였다. 정단부에서 기저부로의 유체 수송은 베스트병 환자 혹은 정상

대조군 역분화줄기세포에 비해 열성유전베스트병 역분화줄기세포에서 더 감소된 소견이 관찰되었다. 유전자 집합 농축 분석 결과, 정상 대조군 혹은 베스트병 환자 역분화줄기세포에 비하여 열성유전베스트병 역분화줄기세포에서 상피간엽이행 유전자 집합 및 NF-κB 경유 TNF-α 신호 유전자 집합의 유의한 농축이 관찰되었다.

결론: 본 연구를 통하여 열성유전베스트병 인간 역분화줄기세포 모델에서 형태학적 이상보다 기능적인 결핍을 확인하였다. 열성유전베스트병은 BEST1 유전자의 변이에 따른 망막색소상피의 기능이상에 의해 발생할 가능성이 있을 것이다.

핵심되는 말 : 열성유전베스트병, 베스트병, 역분화줄기세포, 망막색소상피

PUBLICATION LIST

1. Lee CS, Jun I, Choi SI, Lee JH, Lee MG, Lee SC, et al. A Novel BEST1 Mutation in Autosomal Recessive Bestrophinopathy. Invest Ophthalmol Vis Sci. 2015;56:8141-50.

2. Jun I, Lee JS, Lee JH, Lee CS, Choi SI, Gee HY, et al. Adult-Onset Vitelliform Macular Dystrophy caused by BEST1 p.Ile38Ser Mutation is a Mild Form of Best Vitelliform Macular Dystrophy. Sci Rep. 2017;7:9146.

3. Lee JH, Lee SC, Kim H, Lee CS. COMPARISON OF SHORT-TERM EFFICACY BETWEEN ORAL SPIRONOLACTONE TREATMENT AND PHOTODYNAMIC THERAPY FOR THE TREATMENT OF NONRESOLVING CENTRAL SEROUS CHORIORETINOPATHY. Retina. 2019;39:127-33.

4. Lee JH, Lee SC, Byeon SH, Koh HJ, Kim SS, Lee CS. EFFICACY OF ADJUVANT TOPICAL DORZOLAMIDE-TIMOLOL IN PATIENTS WITH NEOVASCULAR AGE-RELATED MACULAR DEGENERATION REFRACTORY TO ANTI-VASCULAR ENDOTHELIAL GROWTH FACTOR THERAPY. Retina. 2019;39:1953-8.